

ERO2.0 modelling of the effects of surface roughness on molybdenum erosion and redeposition in the PSI-2 linear plasma device

A Eksaeva^{1,8}, D Borodin¹, J Romazanov¹ , A Kreter¹ , A Pospieszczyk¹, S Dickheuer¹ , S Möller¹, B Göths¹, M Rasinski¹ , U Knoche¹, A Terra¹ , A Kirschner¹ , I Borodkina¹, M Eichler¹, B Unterberg¹, S Brezinsek¹ , Ch Linsmeier¹ , E Vassallo², M Pedroni², M Passoni^{2,3} , D Dellasega^{2,3}, M Sala³ , F Romeo³, S Henderson⁴ , M O'Mullane⁵ , H Summers⁵, D Tskhakaya⁶ and K Schmid⁷

¹ Forschungszentrum Jülich GmbH, Institut für Energie- und Klimaforschung—Plasmaphysik, Partner of the Trilateral Euregio Cluster (TEC), Jülich, Germany

² Istituto per la Scienza e Tecnologia dei Plasmi, CNR, Milan, Italy

³ Dipartimento di Energia, Politecnico di Milano, Via Ponzio 34/3, 20133 Milan, Italy

⁴ CCFE, Culham Science Centre, Abingdon OX14 3DB, United Kingdom

⁵ University of Strathclyde, Dept. of Physics, Glasgow G4 0NG, United Kingdom

⁶ Czech Academy of Sciences—Institute of Plasma Physics, Prague, Czech Republic

⁷ Max-Planck-Institut für Plasmaphysik, D-85748 Garching, Germany

E-mail: a.eksaeva@fz-juelich.de

Received 11 July 2019, revised 29 October 2019

Accepted for publication 15 November 2019

Published 16 March 2020



CrossMark

Abstract

The surface morphology of plasma-facing components (PFCs) and its evolution during plasma irradiation has been shown to have a significant effect on the erosion and subsequent transport of sputtered particles in plasma. This in turn can influence the resulting lifetime of PFCs. A model for treatment of the effect of surface roughness on the erosion of PFCs has recently been incorporated into the three-dimensional Monte Carlo code ERO2.0. First simulations have confirmed a significant influence of the assumed surface roughness (for both regular and stochastic numerically constructed samples) on both the effective sputtering yields Y_{eff} and the effective angular distributions of sputtered particles. In this study, a series of experiments at the linear plasma device PSI-2 are conducted to test the effect of surface roughness on the sputtering parameters. Graphite samples prepared with a 100 nm molybdenum layer with various surface roughness characteristic sizes ($R_a = 110$ nm, 280 nm, 600 nm and $R_a < 20$ nm) were exposed to a helium plasma in the PSI-2 linear plasma device at a magnetic field $B = 0.1$ T. These PSI-2 experiments were simulated using ERO2.0 with a surface morphology model. Simulations are able to reproduce the experimentally observed significant suppression of erosion for higher R_a values.

Keywords: surface morphology, 3D Monte Carlo ERO, sputtering, linear plasma device, molybdenum, surface roughness, ERO2.0

(Some figures may appear in colour only in the online journal)

⁸ Author to whom any correspondence should be addressed.

1. Introduction

Erosion of plasma-facing components (PFCs) determines their lifetime and affects other plasma–surface interaction (PSI) issues important for ITER [1], such as impurity sources, tritium (T) co-deposition with beryllium (Be) or material migration [2]. Surface morphology is shown to have a significant effect on sputtering parameters such as effective sputtering yield (Y_{eff}) and angular distributions of the sputtered particles [3, 4], thus erosion determines the preferential areas of erosion and deposition [5]. The influence of developing surface morphology on the Y_{eff} and transport of sputtered particles has been observed in several experiments [6–8]. Some earlier modelling attempts reproduced a decrease of Y_{eff} for a non-smooth surfaces as well as modification of the sheath potential distribution near the rough surface [9–11]. The three-dimensional (3D) Monte Carlo code SURO [12] was coupled with particle-in-cell simulations of the edge plasma in fusion reactors and showed a significant influence of the evolving surface morphology during irradiation on the physical sputtering yield. The recently developed SDTrimSP-3D code was successfully used to simulate the temporal evolution of regular surface structures under ion-beam exposure [13]; however, these approaches and the dedicated validation experiment do not include plasma effects such as the influence of the sheath on ion movement close to the rough surface or local transport of the sputtered particles, which may lead to an additional re-erosion.

The 3D Monte Carlo code ERO [14] is an established tool for modelling the PSI and local impurity transport in a plasma. It considers a wide range of physical processes such as physical sputtering of PFCs and transport of sputtered impurities in the plasma (including ionization, recombination, light emission, plasma friction, elastic collisions, etc.). Moreover, it is capable of modelling widely used diagnostics such as passive optical spectroscopy or deposition on the quartz microbalance (QMB) sensor plate, which allows direct simulation of the experimental results. ERO has been applied to toroidal devices, for example ITER [15] or JET [16], as well as to linear devices such as PSI-2 [6], PISCES-B [17] and Pilot-PSI [18]. Recently an upgraded version of the code—ERO2.0 [19]—was developed. It uses mostly the same physics as the previous version of ERO, but includes massive parallelization, providing the capability to simulate a large number of test particles. ERO2.0 is also capable of processing large and complex 3D-shaped surface geometries, for instance the full ITER and JET-ILW first wall [15, 19]. In our previous work [20] we applied the same ERO2.0 code for the first time to the molybdenum (Mo) rough surface on the micro-scale and simulated the effect of surface roughness on the erosion of several numerically constructed surfaces. It was shown that sharper (more ‘filigree’) surface structures (both regular and irregular) lead to a significant suppression of erosion, for instance up to factor of five to six in the case considered in that work. The present study focuses on experimental validation of this model in experiments in the PSI-2 linear plasma device. Development of a new module for ERO2.0 responsible for the rough surface representation should allow

modelling on the micrometer and machine scales to be combined in the future. The effective sputtering parameters of the rough surface can be derived from micrometer-scale calculations and later be applied as an input for machine-scale simulations.

Linear plasma devices, for example PSI-2 [21], PISCES-B [17] or Pilot-PSI [18], are a perfect testbed for investigating PSI processes due to their simple (compared with tokamaks) geometry and continuous operation. All three mentioned devices provide close to mono-energetic incidence of plasma ions, with the incident energy (E_i) controlled by the bias voltage (U_b) applied to the target. The magnetic field $B \approx 0.1$ T is normal to the target. In this study we test the effect of surface roughness on the erosion by irradiating several Mo-deposited samples with various surface roughness by a helium (He) plasma in the PSI-2 linear device. Moreover, this experiment is dedicated to validate the developed ERO2.0 surface morphology model. In this work we aim to investigate the effect of surface roughness on Y_{eff} , the angular distribution of sputtered particles and the temporal evolution of the surface.

2. ERO2.0 surface morphology model

The rough surface is represented in ERO2.0 by a polygonal mesh of surface cells. Each individual cell is assumed flat and smooth (the sputtering yield and the angular distribution of sputtered particles are calculated using the local incidence angle of the plasma flux constant within the cell). The calculated number of eroded atoms in each cell is distributed between the number of test particles, which are traced later on by ERO during their transport in the local plasma volume until they escape it or hit the wall. Each test particle generated and traced in ERO is a super-particle, consisting of many ‘real’ atoms (the particle weight depending on the modelling case). ERO considers the PSI from each surface collision, which includes sputtering (e.g. physical, chemical) of the target material and reflection or deposition of the incident particle. In this study, about 5×10^5 test particles (about per cell) were traced on each time step. Particles that finally escape from the surface (e.g. not deposited on the neighbouring structures) define the effective sputtering parameters of the rough surface. Various numerical surface topographies can be constructed in ERO2.0: the surface shape can be defined by a formula or randomly generated as a 3D surface mesh with, for example, a certain fractal dimension value D_{fract} . Furthermore, realistic topographies based on atomic force microscopy (AFM) [22] measurements can also be used. The local surface angle with the magnetic field η (determining the dominant incident plasma ion direction) can vary significantly along the rough surface affecting the angular and energy distributions of sputtered particles on the slopes of fine surface structures on the rough surface. It is natural to use η as parameter for sampling these distributions, as has already proved to be useful on the macroscale [23].

It was shown experimentally and in simulations that in the case of oblique ion incidence, sputtered particles tend to

keep the direction of the sputtering ions, at least the velocity component, parallel to the surface plane [24]. The significance of this effect was discussed in our previous study [20]. It was shown that this effect can reduce the resulting Y_{eff} value by $\sim 20\%$.

Currently, there are two possibilities for sampling the energy and angular distributions of sputtered particles in ERO2.0. The first, an analytical approach, is described in detail in our previous work [20]. In this case both polar $f(\theta)$ and azimuthal $f(\varphi)$ angular distributions are sampled independently according to the analytical formula (e.g. a ‘butterfly’ shape for $f(\theta)$ [25]). The energy distribution is sampled according to the Thompson distribution [24] and the sputtering yield value is defined using the Eckstein approximation formulae for the SDTrimSP calculations [26]. Another option implemented recently in ERO2.0 is direct input from the SDTrimSP code [27]. SDTrimSP calculations provide table data on the sputtering yields with the energy and angular distributions of sputtered particles resolved by the incident ion energy E_{in} and angle α . SDTrimSP simulations are conducted for many combinations of materials, and these multi-dimensional data are interpolated during an ERO2.0 run. This method reduces the effort required to search for an appropriate analytical approximation of $f(\theta)$ and $f(\varphi)$, providing the information directly. The downside of this approach, however, is the need to conduct large numbers of SDTrimSP runs before the simulation to prepare a fine enough E_{in}/α mesh. In this work, to maximize precision we use direct input from SDTrimSP; however, it should be noted that this approach can be too time-consuming and require too many data to be used in a general case.

3. Validation of the ERO2.0 surface morphology model

In a previous study [20] we tested the influence of various surfaces by applying ERO to the following two constructed surfaces: 3D cosine peaks and randomly generated fractal surfaces with a given fractal dimension D_{fract} . In the first case Y_{eff} decreased with increase in the aspect ratio of the periodic peaks (height to width ratio). At the same time the angular distribution of the sputtered particles peaked in the direction normal to the surface. A similar effect was observed for the randomly generated surface with the growth of D_{fract} . In both cases a decrease of Y_{eff} by a factor of about two to five was observed in the simulated range of parameters.

The surface evolution under plasma irradiation is treated in ERO2.0 in the following way. For each surface cell the amount of sputtered/deposited material is calculated. These values are transformed into the sputtered/deposited thickness, with sputtering as a negative contribution and deposition as a positive one. For every vertex a weighted average of sputtered thickness values from all its neighbouring faces is calculated and the unity vector of the shift direction is estimated as a weighted average of the normal vectors of the neighbouring faces. After that, normal vectors and areas of all surface cells are recalculated based on the new vertex positions. A

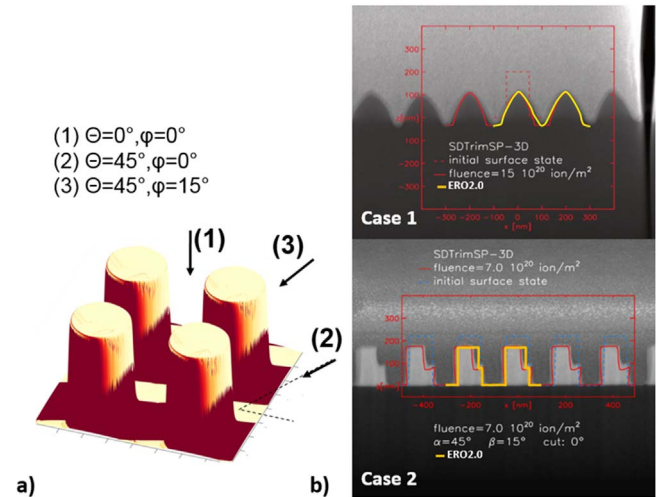


Figure 1. (a) Shadowing pattern calculated in ERO2.0 for the case (3) of inclined Ar ion-beam incidence. The three incidence angle cases are marked as (1), (2), (3). (b) ERO2.0 simulation results for two cases from the ion-beam experiments [14], along with a comparison with SDTrimSP-3D and experimental SEM measurements. Case 1: Ar → Si 5 keV, normal incidence (fluence = $15 \times 10^{20} \text{ m}^{-2}$); Case 2: Ar → Ta 5 keV, $\theta = 45^\circ$, $\varphi = 15^\circ$ (fluence = $7 \times 10^{20} \text{ m}^{-2}$).

triangular mesh was used for the simulations described. Instabilities like overcrossing of two neighbouring faces (an example is the border between the top and the side surface of cylinders considered below) are concealed by removing these faces and a corresponding vertex. This reflects the fact that during the sputtering the total amount of material decreases. In order to avoid artifacts connected to sensitivity of sputtering yields to the surface slope an additional smoothing procedure was applied: the position of each vertex is calculated as an average of the positions of its neighbours (vertices connected to it through a face).

The results of recently conducted ion-beam experiments [13] were utilized to test the ERO2.0 surface modification algorithm. These experiments complement the plasma irradiation experiment discussed below because they allow us to exclude other irradiation processes typical for the plasma (surface sheath E -field, angular and energy distributions of incident ions) apart from the physical sputtering itself. In these experiments silicon (Si) or tantalum (Ta) cylindrical columns (diameter $D = 100\text{--}130 \text{ nm}$, height $H = 200 \text{ nm}$) were exposed to an argon (Ar) ion beam of energy 5 keV. Three ion incidence directions were considered: normal to the target surface (*i.e.* $\theta = 0^\circ$, $\varphi = 0^\circ$), $\theta = 45^\circ$, $\varphi = 0^\circ$ and $\theta = 45^\circ$, $\varphi = 15^\circ$ (see figure 1(a)). This surface morphology was reproduced in ERO2.0 using a polygonal mesh with 500×500 cells, representing an area of $400 \text{ nm} \times 400 \text{ nm}$ ($\approx 0.64 \text{ nm}^2$ cells, with seven to nine atoms in each surface cell). Sputtered particles (5×10^5 test particles, $\approx 3.5 \times 10^5$ ‘real’ atoms in each) were traced in a simulation volume of $400 \text{ nm} \times 400 \text{ nm} \times 210 \text{ nm}$ with periodic boundary in both horizontal directions. Particles that encountered the structures were considered as deposited (100% sticking) with a respective effect on the surface evolution. Reflection was

considered during the runs; however, for some energies of the sputtered Si/Ta (<10 eV) the reflection coefficients were negligible. The incident beam ions were not traced individually but treated as a homogeneous flux, but with a correction to account for self-shadowing by the surface structures. Since the surface topography experienced significant evolution, the shadowing pattern was updated each time step (see figure 1(a)). For the ERO2.0 validation we used (1) the case with Ar ions beam normal to the Si cylinder surface (after fluence $F = 15 \times 10^{20} \text{ m}^{-2}$) and (2) the more complex case of $\theta = 45^\circ$, $\varphi = 15^\circ$ Ar incidence on Ta structures (after fluence $F = 7 \times 10^{20} \text{ m}^{-2}$). Comparison of experimental profiles with the respective ERO2.0 simulations is shown in figure 1(b). One can see that they are in a good agreement for both Si and Ta.

4. PSI-2 experiments on surface roughness: influence on erosion

PSI-2 is a linear plasma device with a magnetically confined (magnetic field $B = 0.1$ T, normal to the target) plasma column of approximately 6 cm diameter. Incident plasma ion energies can be controlled by the bias potential U_b applied to the target. Mass loss measurements of the target provide information about the net erosion, while optical spectroscopy measurements near the target surface can help to estimate the gross erosion and give an insight into transport properties such as impurity penetration length or population evolution of metastable levels [6]. A QMB deposition sensor is installed at a distance of 30 cm from the target along the facility axis outside the plasma column, providing information about the angular distribution of sputtered particles [28]. When interpreted with the ERO modelling, these experiments are capable of giving an understanding of particular PSI and impurity transport processes. In the case at hand, however, the He \rightarrow Mo sputtering was too low to produce any significant deposition on the QMB, therefore this diagnostic is not considered.

For the experiments, samples with various pre-defined roughness values (R_a) were used. An etching procedure was utilized to produce graphite samples of $1 \text{ cm} \times 1 \text{ cm}$ with a rough surface of $R_a = 110 \text{ nm}$, 280 nm , 600 nm and a smooth reference of $R_a < 20 \text{ nm}$ (estimated by AFM) [29]. After the etching, a 100 nm layer of Mo was deposited by pulsed laser deposition [30] on the samples. Thanks to the high energy of this deposition technique, a compact layer is grown mimicking the underlying substrate roughness. The scanning electron microscopy (SEM) [31] pictures of the samples before the exposure are shown in figure 2(a). Two main effects were investigated in the experiments: (a) the influence of surface roughness on Y_{eff} ; (b) the influence of surface roughness on the effective angular distribution of sputtered particles.

The scheme of the experiments is shown in figure 3. Irradiation of several samples simultaneously was achieved using a tungsten (W) target holder with eight slots for $1 \text{ cm} \times 1 \text{ cm}$ samples placed radially symmetrically as shown

in figure 3(a). The profiles of the plasma parameters at PSI-2 have a specific ‘hollow’ shape (minimum plasma temperature T_e and density n_e at the facility axis, maximum at $r \approx 2.5 \text{ cm}$) due to the cylindrical plasma source (figure 3(b)). As shown in figure 3(a), the samples were positioned in the area of maximum flux and all experienced similar exposure conditions. Helium was chosen as the plasma species for these experiments, as the He \rightarrow Mo sputtering yield is comparatively high at low incident energies E_i ($Y_{\text{He} \rightarrow \text{Mo}} \approx 0.001$ for $E_i = 90 \text{ eV}$), while W is not sputtered at all. Moreover, it was important to understand whether the thin Mo layer would be sputtered by the impurities present in the plasma (mainly oxygen). First, to minimize the oxygen (O) content in the plasma we tried to reduce the probability of O desorption during the exposure due to sample heating by outgassing the samples at 300°C before the experiment. Furthermore, the typical amount of O in the PSI-2 plasma is about 0.3%, which can lead to additional erosion of Mo and sputtering of W. In the experiments we used $U_b = -100 \text{ V}$, which after subtracting the plasma potential $U_{\text{plasma}} \approx -10 \text{ V}$ resulted in a He⁺ impact energy of $E_i \approx 90 \text{ eV}$. This is slightly above the sputtering threshold for O \rightarrow W sputtering ($Y_{\text{O} \rightarrow \text{W}} = 0.01$ for the O⁺ of $E_i = 90 \text{ eV}$ impact), and the sputtering yield for O \rightarrow Mo sputtering is $Y_{\text{O} \rightarrow \text{Mo}} = 0.04$, which results in only a 5% contribution of O to the total Mo erosion due to He sputtering and a negligible amount of sputtered W.

In the first experiment eight samples (two identical groups, four various surface roughness values in each of them) were irradiated for 40 min up to a fluence $F = 3.4 \times 10^{24} \text{ m}^{-2}$ in order to measure Y_{eff} . The average values of plasma parameters during the exposure were $n_e \approx 3 \times 10^{11} \text{ cm}^{-3}$ and $T_e \approx 5 \text{ eV}$, $U_b \approx -100 \text{ V}$. Samples with identical roughness values were placed at opposite sides of the ‘circle’ in order to take into account possible asymmetry of the plasma column. The mass loss measurements of the samples were conducted after the irradiation. The results are presented in the figure 4. One can see that the measured sputtering yield is smaller for larger R_a values. The lowest Y_{eff} is observed for the highest roughness value (600 nm) and is lower by a factor of 1.5 than for the smooth reference case ($R_a < 20 \text{ nm}$). The dashed red line is the sputtering yield obtained using the Eckstein approximation formula for the SDTrimSP calculations [26]. One can see that even for the smooth case with $R_a < 20 \text{ nm}$ the measured sputtering yield is approximately 1.5 times lower than the SDTrimSP prediction. This had already been observed in previous PSI-2 experiments on W sputtering [6]. The most probable reason for this disagreement is the high uncertainty of the binary collision approximation at these energies [32].

In the second experiment the penetration length of the sputtered Mo and its possible alterations during the exposure were measured for each type of roughness. For that six out of eight graphite–Mo samples were replaced by W placeholders. Two Mo samples had the same roughness value and were positioned opposite each other (see figure 3(c)). The spectrometer measured Mo I $\lambda = 386.4 \text{ nm}$ light emission profiles along the facility axis at . The spectrometer view was directed across the plasma column covering both Mo samples, therefore the emission intensity was doubled. The experiment

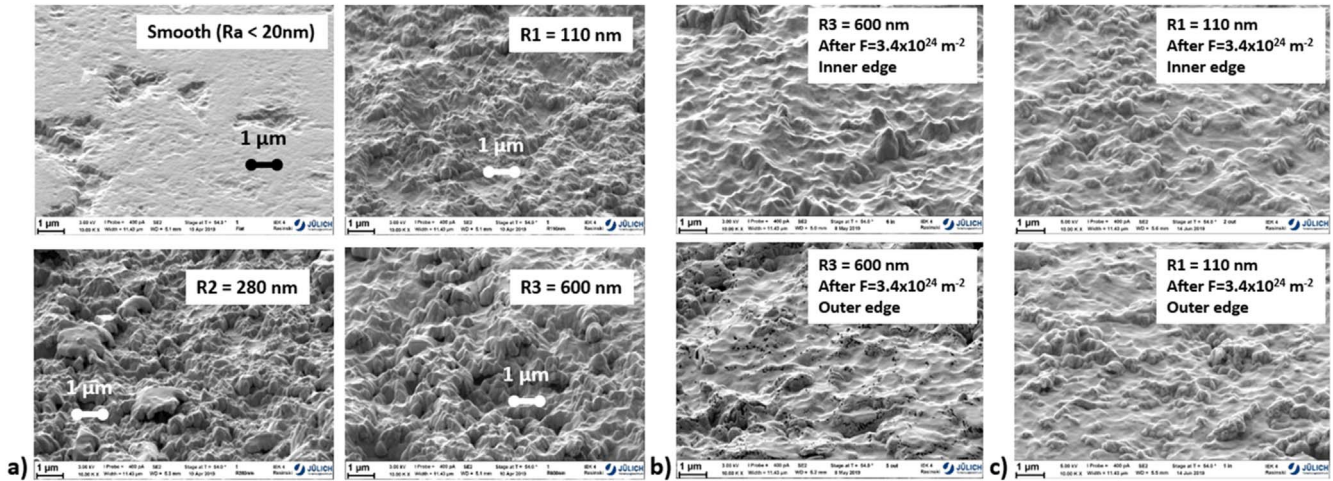


Figure 2. SEM measurement results for the rough surfaces. (a) Before exposure, all roughness cases. (b) Roughness case $R_3:R_a = 600$ nm after He plasma exposure with fluence $F = 3.4 \times 10^{24} \text{ m}^{-2}$; ‘outer’ edge of the sample and ‘inner’ edge of the sample (see figure 4). (c) Roughness case $R_1-R_a = 110$ nm after He plasma exposure with fluence $F = 3.4 \times 10^{24} \text{ m}^{-2}$; ‘outer’ edge of the sample and ‘inner’ edge of the sample.

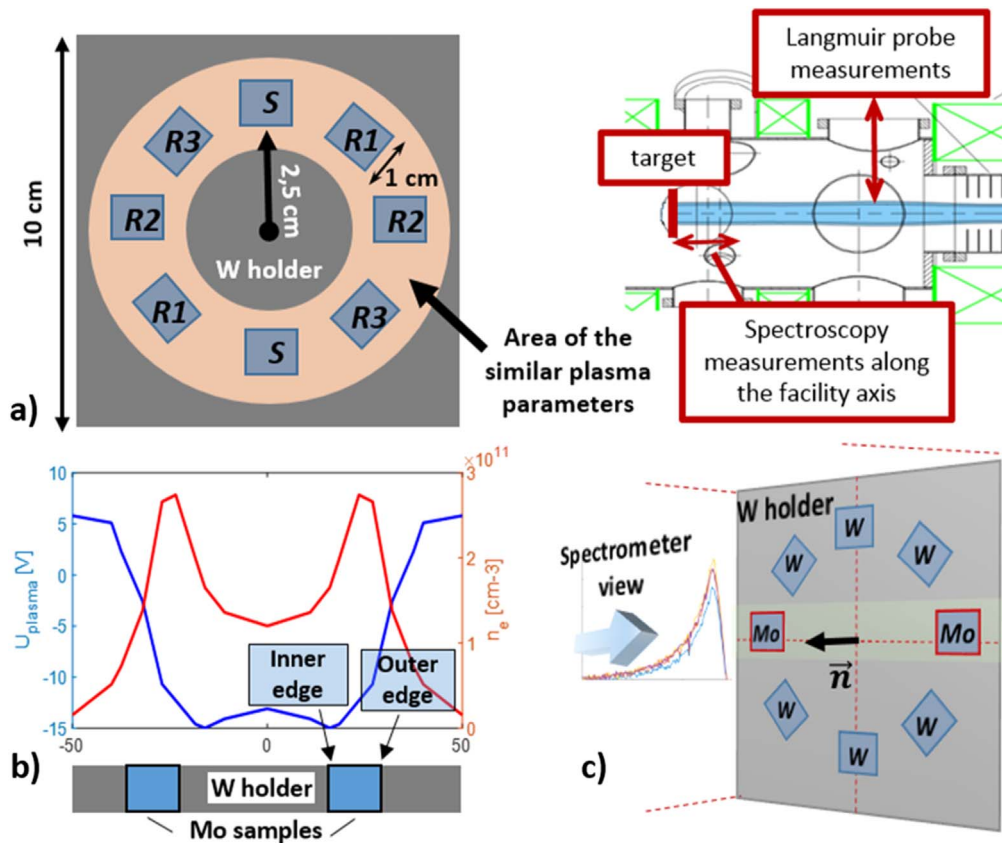


Figure 3. (a) Left: target configuration—the W sample holder with samples of various roughness types (S, smooth, $R_a < 20$ nm, $R_1-R_a = 110$ nm, $R_2-R_a = 280$ nm, $R_3-R_a = 600$ nm). Right: part of the PSI-2 scheme near the target with the spectroscopy measurement area marked. (b) PSI-2 plasma density and plasma potential profiles with the samples marked. (c) Target configuration for the second experiment with two Mo samples of the same R_a (the experiment was conducted for each R_a value).

was repeated four times for $R_a = 110$ nm, 280 nm, 600 nm and $R_a < 20$ nm. During the plasma irradiation (≈ 40 min) both absolute light emission intensity and penetration depth ξ of Mo in the plasma stayed stable ($\xi = 10.5 \pm 1.0$ mm). Moreover, no visible changes were observed between various roughness cases. The minor variations observed in the

absolute value of the light emission intensity were due to slow alterations of the plasma flux, since the ratio between the Mo I line $\lambda = 386.4$ nm and the He I line $\lambda = 388.8$ nm intensities stayed the same.

Moreover, SEM analysis after all exposures showed that the surface topography remained the same during the

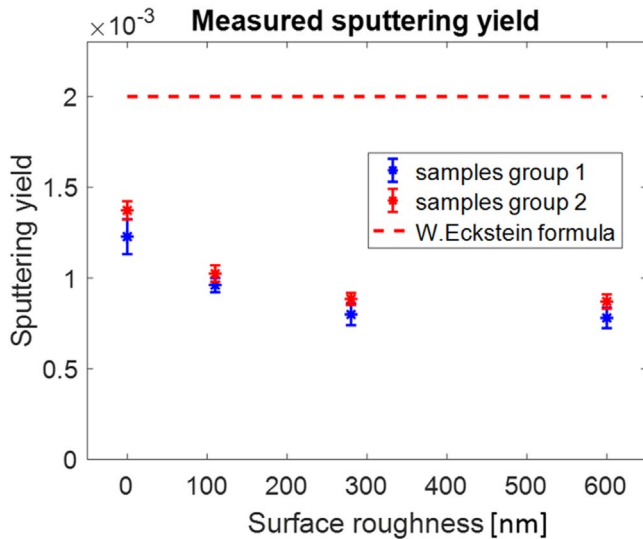


Figure 4. Effective sputtering yield Y_{eff} measured in the PSI-2 experiments for surface roughnesses $R_a = 110$ nm, 280 nm, 600 nm and a smooth reference with $R_a < 20$ nm (He \rightarrow Mo irradiation, $E_{\text{in}} \approx 90$ eV). The red dashed line is the Eckstein [24] sputtering yield value.

irradiation for the case of $R_a = 600$ nm (see figure 2(b)). This result is expected, since the layer of deposited Mo was only 100 nm and the plasma parameters were chosen so as to avoid its complete sputtering during the irradiation. Therefore, one could not expect to see significant changes to the surface on the scale of 100 nm. At the same time, partial smoothing of the surface is visible for the case with the $R_a = 110$ nm (see figure 2(c)). All SEM pictures were taken on two sides of the sample—the inner side of the circle and the outer one. The reason for this is the uneven distribution of plasma parameters over the sample. One can see in figure 3(b) that U_{plasma} changes significantly in this region, which leads to the variations of E_i by $\approx 5\%$. Furthermore, opposite sides of the sample experience different fluxes. One can notice black dots present on the inner side, which was subjected to a higher flux, even though the topography looks similar for the inner and outer sides of the sample. The Rutherford backscattering (RBS) analysis confirmed that the Mo layer was eroded unevenly over the sample; however, it was not eroded completely (e.g. for the smooth case the lowest observed thickness of the Mo layer was ≈ 30 nm). Therefore, it is most likely that the black dots observed are holes produced by the desorption of O from the C substrate.

5. ERO2.0 simulation of the PSI-2 surface roughness experiments

In order to get an understanding of the interplay between processes contributing to the erosion of the samples, ‘machine-scale’ ERO2.0 modelling was conducted. The aim of this modelling was to track processes such as sputtering of target materials (Mo, W) by plasma impurities (O) or

redeposition of W/Mo on the rough Mo surface. Moreover, due to the uneven distribution of plasma profiles over the sample it was important to estimate the distribution of the net erosion value over the sample surface. ERO2.0 confirmed the expected result: O sputtering contributes less than 5% to the total erosion of the Mo samples and the difference between the net and gross erosion values integrated over the sample is less than 1%. The redeposition of W on the sample surfaces is negligibly small according to ERO2.0. This is also confirmed by the RBS measurements, which showed a < 0.15 nm layer of W on all the samples. The distribution of the net erosion value over the sample surface is shown in figure 5(a). One can see that it is quite uneven over the sample surface with the maximum in the central part of it. This is in line with visually observed changes of the sample surface and the RBS measurements (see figures 5(b), (c))—the dark area resulting from higher incident fluence is visible on the sample and RBS measurements have shown that the Mo layer is thinner in the centre of the sample than on the edges.

The ‘micro-scale’ ERO2.0 runs were conducted for surface roughness types corresponding to those observed in the experiment. For this the results of AFM measurements [$14 \mu\text{m} \times 14 \mu\text{m}$ using 6.5×10^4 cells or $70 \mu\text{m} \times 70 \mu\text{m}$ using 2.5×10^5 surface cells, therefore roughly $(2-3) \times 10^4$ Mo atoms in the surface cell] have been directly incorporated in ERO2.0 to define the rough surface (see figure 6(b)). Processes such as W and Mo redeposition from the plasma have not been considered as they have been shown to be negligible by the machine-scale runs above and RBS measurements. As before, the sputtered particles have been traced until they leave the simulation volume or are redeposited on the neighbouring structures. A total of 5×10^5 test particles were tracked on every iteration step, each consisting of $\approx 1 \times 10^9$ ‘real’ atoms. The side boundaries of the simulation box were periodic and the simulated area was much smaller than the characteristic size of the plasma parameters gradient. The velocity vectors of the particles leaving the simulation volume through the upper boundary have been recorded as parameters of finally sputtered particles. The values of Y_{eff} of the sputtered particles for considered roughness types are presented in figure 6(a). One can see the maximum decrease of the effective sputtering yield is by a factor of ≈ 1.3 for $R_a = 600$ nm compared with the smooth reference. The effective angular distribution remains the same for various R_a values. This decrease of Y_{eff} is smaller than that measured in the experiment. The possible reason for this is the fact that AFM measurements are not able to catch fine details of the surface topography, especially for cases of high R_a like $R_a = 600$ nm. This can be compared with the reduction of D_{fract} of the surface structures, which in turn leads to a larger Y_{eff} , as was shown in previous studies [20]. Time-resolved ERO2.0 simulations have shown that the surface topography in general stays stable over the exposure time, with only the finest topography structures smoothed away, which is in line with the experimental observations.

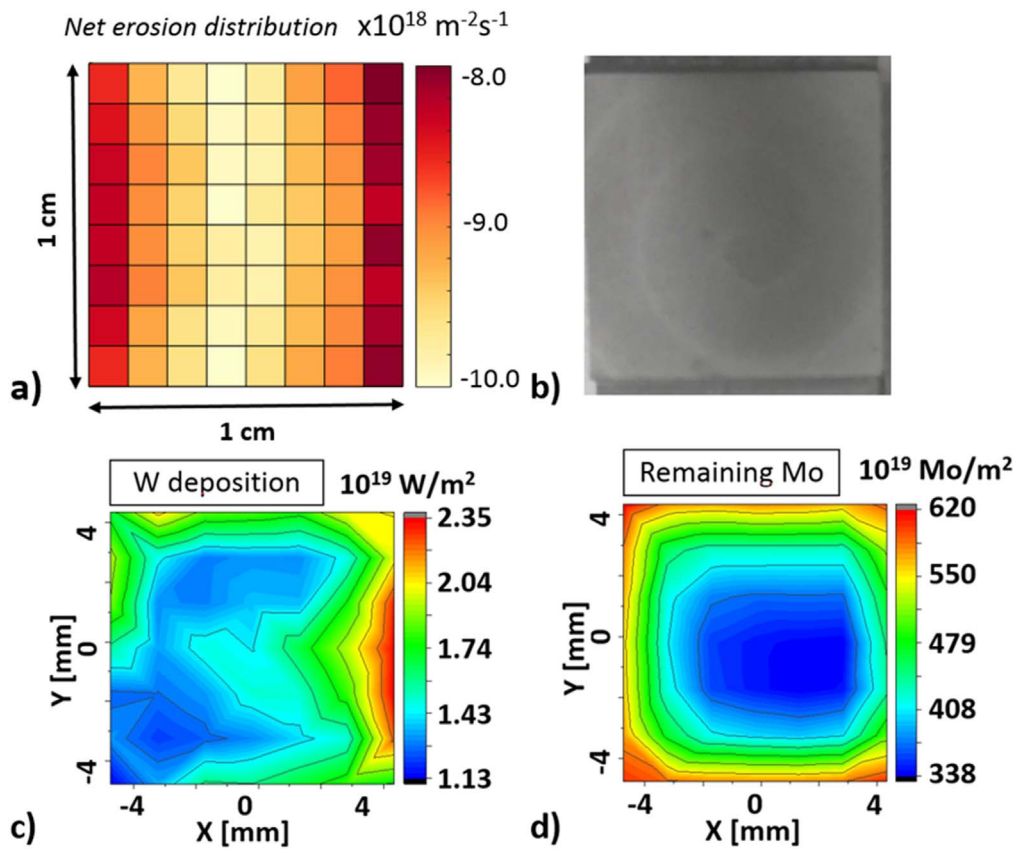


Figure 5. (a) Distribution of net Mo erosion over the sample surface simulated by ERO2.0. (b) Photo of the sample surface with $R_a = 600$ nm after a fluence of $3.4 \times 10^{24} \text{ m}^{-2}$. (c) RBS measurements of the W layer thickness of the sample with $R_a < 20$ nm. (d) RBS measurements of the Mo layer thickness of the sample with $R_a < 20$ nm.

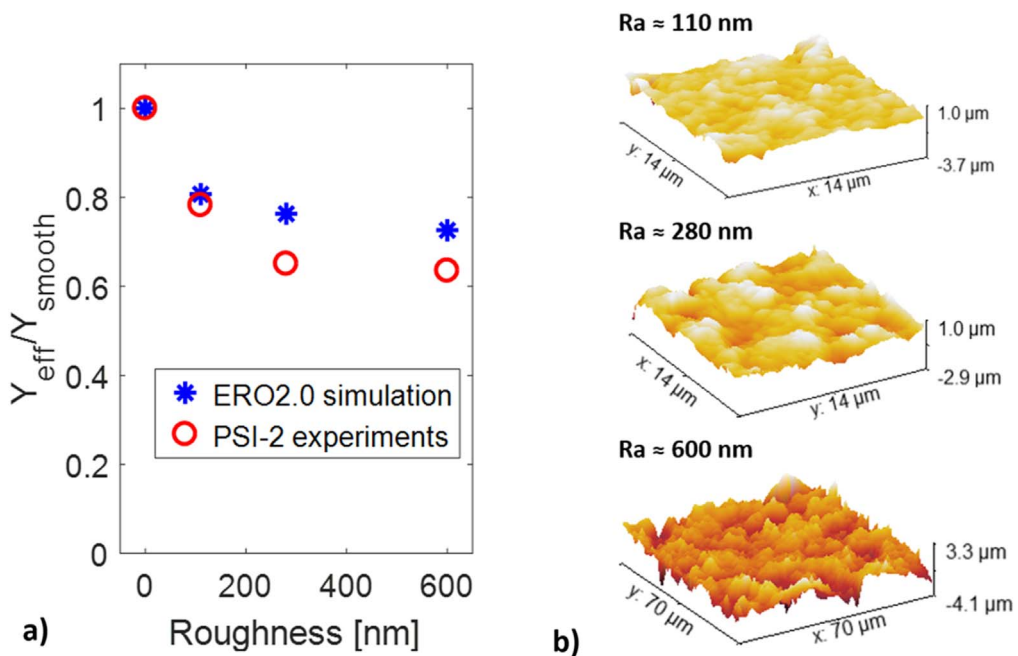


Figure 6. (a) Ratio of Y_{eff} from the rough surface to Y_{smooth} for $R_a = 110$ nm, 280 nm and 600 nm. ERO2.0 simulation results and the measured values from the PSI-2 experiments. (b) Surface topography for $R_a = 110$ nm, 280 nm and 600 nm obtained from AFM measurements.

6. Summary and conclusions

In this work the effect of surface roughness was implemented in the 3D Monte Carlo PSI and plasma impurity transport code ERO2.0. Surface morphology is shown by ERO2.0 simulations to affect the effective sputtering yield Y_{eff} and angular distribution of sputtered particles: sharper (more ‘filigree’) surface structures, both regular and irregular, lead to a suppression of erosion. The surface modification algorithm was validated with ion-beam experiments on high-energy Ar^+ sputtering of cylindrical Si/Ta nanometer-scale structures under various incident angles. ERO2.0 simulation results show reasonable agreement with the corresponding SEM measurements.

Experiments at the linear plasma device PSI-2 were conducted in order to test the influence of surface morphology on Y_{eff} and the effective angular distribution of sputtered particles. Validation of the ERO2.0 modelling with the PSI-2 experiments confirms the main trend: greater roughness of the sample surface leads to a reduced Y_{eff} (e.g. $R_a = 600$ nm leads to a decrease of $\approx 40\%$ compared with the smooth case). In the case at hand, the variation of Mo penetration depth with sample roughness was found to be insignificant; this is due to relatively low aspect ratio of the surface structures. Surface topography evolution during exposure was also negligible during the selected exposure time. Longer exposure of the deposited samples would unavoidably lead to the complete destruction of the Mo layer at some locations and did not conform with the idea of the experiment. Both observations are well in line with the conducted ERO2.0 modelling. Deeper insight into the problem can be obtained with further experiments and simulations using specifically manufactured samples with bulk regular structures on the micrometer scale.

Acknowledgments

This work was carried out within the framework of the EUROfusion Consortium and has received funding from the Euratom research and training programme 2014–2018 and 2019–2020 under grant agreement no. 633053. The views and opinions expressed herein do not necessarily reflect those of the European Commission.

ORCID iDs

J Romazanov  <https://orcid.org/0000-0001-9439-786X>

A Kreter  <https://orcid.org/0000-0003-3886-1415>

S Dickheuer  <https://orcid.org/0000-0002-6826-2715>

M Rasinski  <https://orcid.org/0000-0001-6277-4421>

A Terra  <https://orcid.org/0000-0003-0638-6103>

A Kirschner  <https://orcid.org/0000-0002-3213-3225>

S Brezinsek  <https://orcid.org/0000-0002-7213-3326>

Ch Linsmeier  <https://orcid.org/0000-0003-0404-7191>

M Passoni  <https://orcid.org/0000-0002-7844-3691>

M Sala  <https://orcid.org/0000-0002-6244-7612>

S Henderson  <https://orcid.org/0000-0002-8886-1256>

M O’Mullane  <https://orcid.org/0000-0002-2160-4546>

References

- [1] Brezinsek S 2015 *J. Nucl. Mater.* **463** 11–21
- [2] Mayer M et al 2007 *J. Nucl. Mater.* **363** 101–6
- [3] Hakola A et al 2014 *Phys. Scr.* **T159** 014027
- [4] Kreter A et al 2008 *Plasma Phys. Control. Fusion* **50** 095008
- [5] Schmid K, Mayer M, Adelhelm C et al 2010 *Nucl. Fusion* **50** 105004
- [6] Eksaeva A et al 2017 *Phys. Scr.* **T170** 014051
- [7] Nishijima D et al 2011 *J. Nucl. Mater.* **415** S96–9
- [8] Doerner R P et al 2014 *Phys. Scr.* **T159** 014040
- [9] Brooks J N, Ruzic D N et al 1990 *J. Nucl. Mater.* **176** 278–82
- [10] Quan S et al 2017 *Contrib. Plasma Phys.* **57** 329–35
- [11] Cohen R H et al 2000 *Contrib. Plasma Phys.* **40** 456–70
- [12] Dai S et al 2015 *J. Nucl. Mater.* **463** 372–6
- [13] Arredondo Parra R 2019 Experimental validation of the Monte-Carlo code SDTrimSP-3D PMFC-17
- [14] Kirschner A et al 2000 *Nucl. Fusion* **40** 989
- [15] Borodin D et al 2019 *Nucl. Mater. Energy* **19** 510–5
- [16] Kirschner A et al 2019 *Nucl. Mater. Energy* **18** 239–44
- [17] Borodin D et al 2007 *Phys. Scr.* **T128** 127
- [18] Borodin D et al 2010 *Contrib. Plasma Phys.* **50** 432–8
- [19] Romazanov J et al 2019 *Nucl. Mater. Energy* **18** 331–8
- [20] Eksaeva A et al 2019 *Nucl. Mater. Energy* **19** 13–8
- [21] Kreter A et al 2015 *Fusion Sci. Technol.* **68** 8–14
- [22] Garcia R et al 2002 *Surf. Sci. Rep.* **47** 197–301
- [23] Borodin D et al 2011 *J. Nucl. Mater.* **415** S219
- [24] Betz G et al 1994 *Int. J. Mass Spectrom. Ion Processes* **140** 1–110
- [25] Goehlich A et al 1999 *J. Nucl. Mater.* **266–269** 501–6
- [26] Ecstein W and Behrisch R (eds) 2007 *Sputtering by Particle Bombardment* (Berlin: Springer) 33–187
- [27] Mutzke A, Schneider R, Eckstein W and Dohmen R 2011 *SDTrimSP Version 5.0 IPP Report* 12/8
- [28] Hayderer G et al 1999 *Rev. Sci. Instrum.* **70** 3696–700
- [29] Vassallo E et al 2016 *Thin Solid Films* **603** 173–9
- [30] Dellasega D et al 2012 *J. Appl. Phys.* **112** 084328
- [31] Goldstein J I, Newbury D E, Michael J R, Ritchie N W, Scott J H J, Joy D C et al 2017 *Scanning Electron Microscopy and X-ray Microanalysis* (Berlin: Springer)
- [32] Doerner R P et al 2013 *J. Nucl. Mater.* **438** S272–5